

# 1 Slow strain waves in blocky geological media from GPS and 2 seismological observations on the Amurian plate

3  
4 V.G. Bykov and S.V. Trofimenko

5  
6 Institute of Tectonics and Geophysics, Far Eastern Branch, Russian Academy of Sciences,  
7 65, Kim Yu Chen St., Khabarovsk, 680000, Russia

8 *Correspondence to:* V.G. Bykov (bykov@itig.as.khb.ru)  
9

10 **Abstract.** Based on the statistical analysis of spatiotemporal distribution of earthquake  
11 epicenters and perennial geodetic observation series, new evidence is obtained for the existence  
12 of slow strain waves in the Earth. The results of our investigation allow us to identify the  
13 dynamics of seismicity along the northern boundary of the Amurian plate as a wave process.  
14 Migration of epicenters of weak earthquakes ( $2 \leq M \leq 4$ ) is initiated by the east-west propagation  
15 of a strain wave front at an average velocity of 1000 km/yr. We have found a synchronous quasi-  
16 periodic variation of seismicity in equally spaced clusters with spatial periods of  $3.5^\circ$  and  
17  $7.26^\circ$  comparable with the length of slow strain waves. The geodetic observations at GPS sites in  
18 proximity to local active faults show that in a number of cases, the GPS site coordinate seasonal  
19 variations exhibit a significant phase shift, whereas the time series of these GPS sites differ  
20 significantly from a sinusoid. Based on experimental observation data and the developed model  
21 of crustal block movement we have shown that there is one possible interpretation for this fact  
22 that the trajectory of GPS station position disturbance is induced by migrating of crustal  
23 deformation in the form of slow waves.

24  
25 **Key words:** background seismicity, seismic clusters, strain waves, Amurian plate, space-time  
26 seismicity model, oscillatory movements of crustal blocks.  
27  
28  
29  
30  
31  
32  
33  
34  
35  
36  
37  
38  
39  
40  
41  
42  
43  
44  
45  
46  
47  
48  
49  
50  
51

## 52 **1 Introduction**

53

54 The inhomogeneous blocky structure of the crust and the lithosphere considerably affects  
55 the deformation, seismic, filtration and other processes. The effect of the blocky structure on the  
56 distribution of earthquakes can be especially clearly traced. It is exactly the blocky structure of  
57 the geological medium which results in the generation of waves of different types including  
58 slow strain waves (Bykov, 2008). Clarification of the link between movements of tectonic  
59 structures and slow strain wave processes is of fundamental importance for expanding our  
60 understanding of the physics of earthquakes.

61 The most important problem of recent geodynamics is to clarify the mechanisms  
62 responsible for the propagation of the energy of deformation processes and tectonic stress  
63 transfer at the boundaries between the blocks and the lithospheric plates, and to explore the  
64 causes of migration of earthquake epicenters. The problem has been argued for more than 45  
65 years since Elsasser's publication (1969), suggesting the equation of local stress transfer in the  
66 rigid elastic lithosphere underlain by the viscous asthenosphere. The possibility of using  
67 Elsasser's model to describe migration of seismicity was further discussed in papers published  
68 by other researchers. Bott and Dean (1973) introduced the term "stress or strain waves" and  
69 obtained the expression for the velocity of the wave propagating along the lithospheric plate.  
70 According to their calculation, the stress wave velocity attains to 0.1-100 km/yr. Anderson  
71 (1975) generalized Elsasser's model in order to elucidate the mechanism of earthquake migration  
72 in the subduction zone and estimated the stress wave velocity along the island arc about 50-170  
73 km/yr. In the model developed by Ida (1974), the solution was obtained in the shape of "slow-  
74 moving deformation pulses" propagating along the fault at a constant velocity. The gouge  
75 viscosity and thickness variations in the fault yield the pulse velocity ranging from 10-100 km/yr  
76 to 1-10 km/day. The first interval corresponds to earthquake migration velocities at a wavelength  
77 of about tens of kilometers, whereas the second interval is compliant with aseismic creep at  
78 about 1 km wavelength. Scholz (1977) introduced the concept of the "deformation front" to  
79 describe large-scale tectonic processes triggering large earthquakes. As estimated by Scholz, the  
80 velocity of the deformation front propagating through NE China, that triggered the 1975, M=7.3  
81 Haicheng earthquake, attained to 110 km/yr.

82 The advances in theoretical studies of slow strain waves in the Earth initiated the search  
83 for the possibilities of experimentally detecting the propagation effects of the waves of this type,  
84 and, in the first place, the intense study of earthquake migration. By now, the deformographic,  
85 geodetic and hydrological measurements performed worldwide have revealed the migration of  
86 deformations at velocities of about 10-100 km/yr and 1-10 km/day (Kasahara, 1979; Bella et al.,  
87 1990; Harada et al., 2003; Kuz'min, 2012; Reuveni et al., 2014; Yoshioka et al., 2015).

88 Migration of earthquake epicenters coincides with the velocity (10-100 km/yr) and direction of  
89 crustal deformation movement (Kasahara, 1979; Barabanov et al., 1988) and with hydrological  
90 effects (Kissin, 2008). Furthermore, the absorption and dispersion of the waveforms of  
91 migrating deformation were detected (Kasahara, 1979; Barabanov et al., 1988), i.e., the main  
92 properties of a common wave process. In terms of the physical mechanism of propagation, slow  
93 strain waves are similar to common seismic waves, but the fundamental difference is that they  
94 propagate at super low velocities, ultra low frequencies and have large wavelength (Bykov,  
95 2005). This hampers the direct instrumental measurements of strain waves and the concomitant  
96 effects.

97 In the present study, we have obtained new evidence of the existence of strain waves in the  
98 Earth resting upon a comprehensive statistical analysis of the dynamics of seismicity along the  
99 northern boundary of the Amurian plate and the data derived from in situ GPS experimental  
100 observations performed near this boundary.

101

## 102 **2 Methods for detection of slow strain waves**

103

104 Slow strain wave transmittance through the fault-blocky geological medium is  
105 accompanied by various seismic, hydrogeological, electrokinetic, geochemical and other effects.  
106 The methods for strain wave detection are divided into indirect, that display the wave-shaped  
107 variations in the geophysical fields due to temporal variations of the stress state of the medium,  
108 and direct ones immediately recording the migration of deformations.

109 The seismic, geoelectric and geochemical methods of strain wave recording are referred to  
110 the indirect methods. Indirect evidence of the existence of strain waves is manifested in the  
111 targeted migration of large earthquakes (Stein et al., 1997), the occurrence of seismic velocity  
112 anomalies (Lukk and Nersesov, 1982; Nevskii et al., 1987), a cyclic wandering of aseismic  
113 strips in the Earth's mantle (Malamud and Nikolaevsky, 1983; 1985); oscillatory movements of  
114 the seismic reflection sites (Bazavluk and Yudakhin, 1993; Bormotov and Bykov, 1999) and the  
115 migration of geophysical field anomalies (radon, electrokinetic signals) in proximity to faults  
116 (Nikolaevskiy, 1998).

117 The direct indications of strain waves are displayed in wave fluctuations of the ground  
118 water level and the migration of slopes and surface deformations. The direct methods exploring  
119 temporal variations of crustal deformation comprise the deformographic (Kasahara, 1979; Ishii  
120 et al., 1983; Nevskii et al., 1987; Bella et al., 1990; Harada et al., 2003), hydrogeodynamic  
121 (Barabanov et al., 1988; Kissin, 2008) and geodetic measurements (Kuz'min, 2012) including  
122 the methods of deformation measurements using laser ranging (Milyukov et al., 2013) and GPS  
123 observations (Reuveni et al., 2014; Yoshioka et al., 2015).

124 To detect the main physical mechanisms of seismicity migration and the generation of  
125 signals of different nature that are accompanying strain waves, we need performing further  
126 observations and improving GPS- and seismological data processing technique, and conducting  
127 theoretically prepared and purposeful experiments.

128 The answer to the question “where to search for slow strain waves?” is directly linked  
129 with the detection of the main types of tectonic structures generating these waves.

130

### 131 **3 Tectonic structures generating slow strain waves**

132

133 From the published results it follows that subduction, collision, active riftogenesis and  
134 transform fault zones are the most probable types of tectonic structures generating strain waves.  
135 These intensive sources of different tectonic nature possess a common property – they are the  
136 interaction zones between crustal blocks and the lithospheric plates.

137 Migration of shear deformation in subduction zones is directed from the ocean toward the  
138 coast. This general tendency was first revealed in area of the Japan island arc where migration is  
139 oriented east-west, and in the opposite Pacific coastal area – in the western Cordilleras, where  
140 deformations migrated from south to north (Kasahara, 1979). Migration of the maximum of the  
141 vertical crustal deformation from the subduction zone toward the continent at a velocity of  
142 about 10 km/yr was also observed near the Tohoku region (northeastern Japan) and the Izu  
143 Peninsula (central Japan), where the Pacific and Philippine plates subduct beneath the Eurasian  
144 plate (Miura et al., 1989). All these data reasonably lead to an assumption that subduction zones  
145 are one of the possible sources of slow strain waves.

146 The seismicity pattern observed in the south of Middle Asia can also be explained by strain  
147 waves excited under the oscillating regime of the Eurasian and Indian lithospheric plate collision  
148 in the Pamir and Tien Shan junction zone (Nersesov et al., 1990). The compression at the  
149 Indostan and Eurasian lithospheric plate boundary in the Himalayan collision zone is the source  
150 of “fast” and “slow” waves of plastic deformation that trigger earthquakes in Central and East  
151 Asia (Wang and Zhang, 2005).

152 In the Baikal rift system, four main groups of strain waves with different velocities (7-95  
153 km/yr) and lengths (130-2000 km) are distinguished that cause recent activation of seismoactive  
154 faults in Central Asia (Gorbunova and Sherman, 2012).

155 Based on continuous long-term seismic and laser ranging observation data, it has been  
156 established the effect of propagation of slow waves of tectonic deformations traveling along  
157 transform faults at velocities of 40-50 km/yr at the lithospheric plate boundaries in Southern  
158 California and the Kopet-Dag region (Nevskii et al., 1987). Seismicity variations along the

159 Pacific and North American plate boundary in the San-Andreas transform fault zone (California)  
160 are also suggested to be associated with “slowly traveling strain waves” (Press and Allen, 1995).

161 The rotational block movements in the fault zones due to tectonic processes or earthquakes  
162 are considered one of the main physical mechanisms of strain wave generation (Nikolaevskiy,  
163 1996; Lee et al., 2009; Teisseyre et al., 2006).

164

#### 165 **4 Seismic effects of slow strain waves at the northern edge of the Amurian plate**

166

167 In order to specifically investigate the relationship between strain waves and the dynamics  
168 and seismicity pattern observed in fault-blocky geological media, we have selected the study  
169 area on the northern margin of the Amurian plate – the most seismically active area of the  
170 interaction zone between the Amurian and Eurasian plates.

171 The analysis of the spatiotemporal seismicity pattern observed in vast regions is commonly  
172 performed based on statistical processing of earthquake catalogues. The directions of earthquake  
173 epicenter (or groups of epicenters) displacements are defined and their displacement rates are  
174 determined. As opposed to the standard regional approach, we here applied a comprehensive  
175 analysis including both conventional statistical methods and those of cluster analysis adapted by  
176 the authors for the geodynamic zone gradation. The details of developed clustering technique  
177 and statistical analysis of background seismicity can be found in (Trofimenko et al., 2015). **In**  
178 **paper by Trofimenko et al. (2016a), statistical validity of the applied method is shown and the**  
179 **correctness of the models is evaluated.**

180 To study the dynamics of seismicity in different zones, the area along the northern  
181 boundary of the Amurian plate was divided into separate clusters (Fig. 1). When clustering, we  
182 applied the criterion of earthquake grouping near active faults, and the geomorphological and  
183 tectonic features of active structures, as well as the presence of meridional (submeridional) first-  
184 rank faults within the distinguished zones, were taken into consideration.

185 When developing space-time models of seismicity, the spatial relationship between  
186 separate seismic clusters during a year was revealed and taken into account. Based on statistical  
187 distributions of earthquakes, the analysis of seismicity maxima passage over east-westerly  
188 arranged clusters has been performed.

189 The basic data were derived from the catalogue “Earthquakes of Russia”  
190 (<http://eqru.gsras.ru>), the catalogue compiled by the Baikal Branch of the Geophysical Survey of  
191 the Russian Academy of Sciences (GS RAS) (<http://www.seis-bykl.ru/>) and the IRIS catalogue  
192 (<http://www.iris.edu>).

193 As a result of the calculation, the average period of seismicity maximum passage in days  
194 from the beginning of the year has been determined for each cluster, which is assigned to the

195 average value of the cluster longitude. These values were used for the calculation of the  
196 displacement rate of seismicity maxima. We calculated the velocities and wavelengths of slow  
197 strain waves from the maxima of the spatial correlation of seismicity.

198 The spatiotemporal distributions of earthquake epicenters reflect synchronization of  
199 seismicity maxima in the annual cycles over a certain spatial interval (migration period). The  
200 statistical calculations performed for each cluster allowed the identification of six similar  
201 spatiotemporal cycles of seismicity maxima migration A, B, C, D, E and F (Fig. 1), for which the  
202 spatial periods of migration and displacement rates of seismicity maxima have been calculated.

203 In the northeastern segment, the maxima of statistical distributions are located in the  
204 clusters arranged nearly equally apart from each other, at  $L_{A-C} = (7.26 \pm 0.74)^\circ$ , which corresponds  
205 to a distance of 360-420 km for a range of investigated latitudes. For the northwestern segment,  
206 the spatial period is equal to  $L_{D-F} = (3.8 \pm 0.5)^\circ$ , at the average, which corresponds to half of the  
207 interval  $L_{A-C}$ , or a distance of 210-270 km (Fig. 1). In the study area, the parameter  $L_{A-C}$  is equal  
208 to double the distance between the main structural-tectonic elements of the Earth's crust and  
209 corresponds to double the size of tectonic inhomogeneities revealed from the geophysical field  
210 anomalies (Trofimenko, 2010).

211 The determined spatial period  $L_{A-C} = 7.26^\circ$  (360-420 km) is comparable with the  
212 wavelength  $\lambda = 250-450$  km of slow strain waves observed in the study area on the northern  
213 margin of the Amurian plate (Pribaikalya and Priamurye areas lying within  $107^\circ\text{E}-140^\circ\text{E}$ )  
214 (Sherman et al., 2011). The direction of the seismicity maxima displacement coincides with the  
215 displacement vector of the strain wave front (Sherman, 2013) (Fig. 2).

216 The displacement rate values for seismicity maxima are obtained from regression  
217 equations using the linear approximation method and are equal to  $U_A = -950$  km/yr,  $U_B = -1170$   
218 km/yr,  $U_C = -986$  km/yr,  $U_D = -953$  km/yr,  $U_E = -1033$  km/yr and  $U_F = -725$  km/yr for spatial cycles  
219 A, B, C, D, E and F, respectively. The minus sign means the westward displacement of the  
220 seismicity maxima.

221 For the entire northeastern segment, the average value of the velocity modulus of the  
222 seismicity maxima displacement (with a relative determination error of 7%) is equal to  $U_{A-C} =$   
223  $1000-1022$  km/yr, whereas for the northwestern segment this value is  $U_{D-F} \approx (913 \pm 110)$  km/yr.  
224 The seismicity maxima displacement rate value is  $U_{A-F} \approx (979 \pm 124)$  km/yr or about 1000 km/yr  
225 along the entire northern boundary of the Amurian plate.

226

## 227 **5 The slow strain wave effects inferred from GPS observations**

228

229 To explore the deformation processes in the geological medium with a discrete blocky  
230 structure and to perform special GPS experimental observations, we selected the South Yakutia



231 geodynamic polygon located near the northern boundary of the Amurian plate, at the junction of  
232 two major tectonic structures – the Aldan Shield and the Stanovoy Range. Recently, a number of  
233 blocks of different size and configuration have been inferred here from geological data. These  
234 blocks experience the vertical and horizontal movements of different directions, velocities and  
235 amplitudes (Imaeva et al., 2012), which are responsible for a complicated character of tectonic  
236 movements.

237 We have analyzed a set of time series obtained at two of collocated GPS sites NRGR and  
238 NRG2 situated near the active fault intersection area in the central part of the Stanovoy Range  
239 (Fig. 1). The NRGR site is located in area of the Chulman depression on 15×20 km<sup>2</sup> size  
240 microblock and is involved in different types of crustal movements and deformations in  
241 consistency with the kinematics of the bordering active faults (Trofimenko and Bykov, 2014).  
242 The site NRG2 location is approximately 2 km south of the NRGR site and closer to the zone of  
243 influence of the active Berkakit fault. The GPS time series obtained at stations NRGR and NRG2  
244 for the horizontal and vertical components are shown in Fig. 3. The stable long-period  
245 displacement component is typical for both observation sites in the southeastern direction. For  
246 the vertical and horizontal components observed in other directions, the course of the annual  
247 displacements is absolutely different. At the two observation sites, the horizontal displacement  
248 components in the “North-South” direction are represented by in-phase curves that can be  
249 approximated by a sinusoid (Fig. 3 a), which is in consistency with the approximation suggested  
250 in Serpelloni et al. (2013). The vertical and horizontal displacement components in the “East-  
251 West” direction vary in an anti-phase manner during separate periods of measurements (Fig. 3 b,  
252 c), which contradicts the common dynamics of long-period components. The shapes of these  
253 curves for the horizontal displacement components are appreciably different from a sinusoid  
254 (Trofimenko et al., 2016b).

255 It is necessary to emphasize that the meteorological factors in the annual cycles influence  
256 the shapes of the movement trajectories of the collocated sites equally (van Dam et al., 1994).  
257 Therefore, the detected paradox cannot be explained by the meteorological causes.

258 This paradox can only be resolved in the case when the observation sites are adjacent to the  
259 boundaries of specific – “hinge” – type local faults (Fig. 4 a). Really, for the site NRGR, a local  
260 feathering fault of the Sunnangyn-Larba northeast-trending fault system is the “hinge”, whereas  
261 for the site NRG2, the “hinge” is one of the branches of the Berkakit northwest-trending fault  
262 (Fig. 1). The physical model of this fault-blocky structure can be represented as a set of rods –  
263 physical pendulums (Fig. 4b), whose lower parts are fixed, while the upper parts are disturbed  
264 from the equilibrium condition. In this case, the upper parts of the rods (blocks) are displaced  
265 with respect to some central line (the fault hinge).

266 The approximation curve fitting for the vertical component of block displacement has led  
 267 to one more unexpected result. The shape of the best fit function approximating the experimental  
 268 curve appeared to coincide with a breather – the solution (2) of the sine-Gordon equation (see  
 269 below). When selecting the theoretical curve in the shape of a breather (2), this result for the  
 270 “North-South” component is obtained at  $\omega = 0.873$  with an error equal to 0.048 (for the sine  
 271 0.069), while for the “East-West” component – at  $\omega = 0.780$  with an error equal to 0.052 (for the  
 272 cosine 0.149). The approximation error of experimental data is calculated from the formula

273 
$$\sigma = \sqrt{1/12 \sum_{k=1}^{12} (Y_k^E - Y_k^T)^2}$$
, where  $Y_k^E - Y_k^T$  are the residuals between the observed and calculated

274 monthly averaged station positions for the sinusoid and breather. The shapes of the fitted curves  
 275 are shown in Fig. 5, for more details see Trofimenko et al. (2016b).

276 The coincidence of the trajectory shape of measured vertical displacements with the shape  
 277 of a breather, and the correspondence of the blocky structure in area of GPS site locations to the  
 278 model of coupled pendulums served as a motivation for application of the sine-Gordon equation  
 279 to describe the evolution of the vertical components of block movements.

280 The mathematical model of quasi-periodical vertical components of oscillations of rigidly  
 281 coupled crustal blocks with the adjacent “hinge”-type faults corresponds to the equation:

282 
$$\frac{\partial^2 \varphi}{\partial \eta^2} - \frac{\partial^2 \varphi}{\partial \xi^2} = \sin \varphi, \quad (1)$$

283 
$$\eta = \omega t, \xi = x\omega/c, \omega^2 = mgl/I, c^2 = \tau d^2/I,$$

284 where  $\varphi$  is the angle of deviation of the pendulum (rod) from the equilibrium position;  
 285  $mgl \sin \varphi$  is the moment of the gravity force,  $m$  is the lamped mass of the pendulum,  $l$  is the  
 286 length of the rod (the height of the block),  $\tau d^2 \frac{\partial^2 \varphi}{\partial x^2}$  is the sum of the moments of the torsion  
 287 forces exerted by the adjacent blocks,  $\tau$  is the constant of the spring torsion (rigidity),  $d$  is the  
 288 increment of the interblock distance (increase or decrease depending on the type of movement),  
 289  $I$  is the moment of the block inertia.

290 One of the solutions of equation (1) is called a breather (dynamic soliton) and represents  
 291 a nonlinear function which, for the case of the soliton with the immobile center of gravity can be  
 292 written as:

293 
$$\varphi(x, t) = 4 \operatorname{arctg} \left[ \left( \frac{\sqrt{1-\omega^2}}{\omega} \right) \frac{\sin(\omega t)}{\operatorname{ch}(x\sqrt{1-\omega^2})} \right], \quad (2)$$



296 where  $\omega$  is the inner frequency of the breather,  $x$  determines the origin of the curve and  $t$  is the  
297 independent variable (time).

298 Like a soliton, the breather has the shape of an impulse; it is localized in space and is  
299 pulsating in time. In the low frequency range  $\omega \ll 1$  the breather can be qualitatively treated as  
300 a weakly coupled kink-antikink pair (the sine-Gordon equation solutions of opposite signs in the  
301 shape of a topological soliton – a wave with a changeless profile in the shape of a kink) (Braun  
302 and Kivshar, 2004).

303 The detected high correlation of the observed site displacement trajectories with the  
304 theoretical curve corresponding to a breather allows us to suggest that the mechanism of these  
305 oscillations can be associated with the occurrence of strain waves in the fault intersection system.  
306 In this case, these waves can be qualitatively treated as standing waves of compression-extension  
307 in the blocky geological medium.

308 The sine-Gordon equation solution in the shape of a breather has previously been applied  
309 for modeling the wave dynamics of faults and strain waves (Mikhailov and Nikolaevskiy, 2000;  
310 Gershenzon et al., 2009; Erickson et al., 2011). Mikhailov and Nikolaevskiy (2000) considered a  
311 scenario when collision of two tectonic waves (kink-antikink collision) resulted in the  
312 occurrence of large earthquake. The solution in the shape of a breather has also been applied for  
313 the interpretation of the features of fault dynamics observed after the 1989 Loma-Prieta  
314 earthquake (Gershenzon et al., 2009). Based on a modified Burridge–Knopoff model, the  
315 solution has been obtained that corresponds to a localized failure – a breather that propagates  
316 along a fault and is damping in the fault segment of the final length (Erickson et al., 2011). Wu  
317 and Chen (1998) have earlier reduced a one-dimensional Burridge–Knopoff spring-block model  
318 to the sine-Gordon equation and applied its solution in the shape of a solitary wave (kink) to  
319 investigate earthquakes.

320

## 321 **6 Concluding remarks**

322

323 The accumulated facts indicate to the propagation of slow wave-like movements within the  
324 crust and the lithosphere at different velocities on global and regional scales (Bykov, 2014). The  
325 results of our investigation (the periodicity of the seismic components, spatial cycles with phase  
326 shift of seismicity maxima, migration velocity of earthquake epicenters) and their comparison  
327 with the known data allow us to identify the dynamics of seismicity along the northern boundary  
328 of the Amurian plate as a wave process. We have revealed synchronous quasi-periodic seismicity  
329 variations in equally spaced clusters with spatial periods of  $7.26^\circ$  and  $3.5^\circ$ , that are comparable  
330 with the length of slow strain waves ( $\lambda=250-450$  km), detected in the Eurasian and Amurian

331 tectonic plate interaction area (107°E-140°E) (Sherman, 2013). The slow strain wave velocity in  
332 Pribaikalya and Priamurye attains to 5-20 km/yr and is comparable with the migration velocity  
333 of crustal deformations (10-100 km/yr) from the Japan-Kuril-Kamchatka subduction zone (Ishii  
334 et al., 1978; Kasahara, 1979; Yoshioka et al., 2015).

335 The calculated average displacement rate value of the maxima of weak seismicity ( $2 \leq M \leq 4$ )  
336 along the northern boundary of the Amurian plate is about 1000 km/yr, which is two orders of  
337 magnitude larger than the velocity of slow strain waves (~10-100 km/yr). This may imply that  
338 slow strain waves modulate variations of weak seismicity ( $2 \leq M \leq 4$ ) during the year.

339 The displacement of seismicity in the annual cycles occurs from east to west and coincides  
340 with the direction of migration of large earthquakes, strain wave fronts and crustal deformation  
341 detected from direct deformographic and GPS measurements (Kasahara, 1979; Bella et al., 1990;  
342 Harada et al., 2003; Yoshioka et al., 2015). The slow strain wave fronts are triggers of large  
343 earthquakes ( $M > 6$ ) in the submeridional faults of the Amurian plate.

344 The spatial correlation of migration of seismicity and deformations as well as the migration  
345 of deformations – two different manifestations of the geodynamic process – may mean that  
346 seismicity migration is associated with the propagation of tectonic stresses in the form of slow  
347 strain waves that cause a complementary load and subsequent earthquake occurrence. The  
348 numerous results of observations of seismicity migration are hard to explain by other causes  
349 rather than wave-like variations of the global and local stress fields.

350 The conclusions on the wave pattern of the deformation process are consistent with the  
351 results of special experimental observations performed to explore crustal block interaction. The  
352 seasonal course of displacements of GPS stations NRGR and NRG2, involved in the in situ  
353 experimental observations, or of the deformations of the blocky structure of the crust, exhibits a  
354 wave-like rather than a linear pattern. The wave-like displacements can be explained by  
355 transmittance of slow strain waves.

356 Resting upon the statistical modeling, we have established the in-phase and anti-phase  
357 changes of the components of the full displacement vector, the relative time delay of the maxima  
358 and minima for separate components, and dissimilarity of the displacement trajectory from a  
359 sinusoid. In order to describe the evolution of oscillations of the interacting blocks, a simple  
360 mathematical model is proposed from which it follows the explanation of the observed specific  
361 behavior of these blocks.

362 Based on experimental observation data and the developed model of crustal block  
363 movement, we have shown that there is one possible interpretation for this fact that the trajectory  
364 of GPS station position disturbance is induced by migrating of crustal deformation in the form of  
365 slow waves.

366 *Acknowledgements.* The reported study was funded by RFBR according to the research project  
367 No. 16-05-00097 a.

368  
369  
370

371 **References**

372

373 Anderson, D.L.: Accelerated plate tectonics, *Science*, 187, 1077-1079, 1975.

374 Barabanov, V.L., Grinevsky, A.O., Kissin, I.G., and Mil'kis, M.P.: Hydrogeological and seismic  
375 effects of deformational waves in the foremost Kopet Dag fault zone, *Izvestiya Akademii*  
376 *Nauk SSSR. Fizika Zemli*, 5, 21-31, 1988.

377 Bazavluk, T.A. and Yudakhin, F.N.: Deformation waves in Earth crust of Tien Shan on  
378 seismological data, *Dokl. Akad. Nauk*, 329, 565-570, 1993.

379 Bella, F., Biagi, P.F., Caputo, M., Della, Monica G., Ermini, A., Manjgaladze, P., Sgrigna, V.,  
380 and Zilpimian, D.: Very slow-moving crustal strain disturbances, *Tectonophysics*, 179, 131-  
381 139, 1990.

382 Bormotov, V.A. and Bykov, V.G.: Seismological monitoring of the deformation process,  
383 *Geology of the Pacific Ocean*, 16, 981-994, 2001.

384 Bott, M.H.P. and Dean, D.S.: Stress diffusion from plate boundaries, *Nature*, 243, 339-341, 1973.

385 Braun, O.M. and Kivshar, Y.S.: The Frenkel-Kontorova model: concepts, methods, and  
386 applications, Berlin: Springer, 2004.

387 Bykov, V.G.: Strain waves in the Earth: Theory, field data, and models, *Russian Geology and*  
388 *Geophysics*, 46, 1158-1170, 2005.

389 Bykov, V.G.: Stick-slip and strain waves in the physics of earthquake rupture: experiments and  
390 models, *Acta Geophysica*, 56, 270-285, 2008.

391 Bykov, V.G.: Sine-Gordon equation and its application to tectonic stress transfer, *Journal of*  
392 *Seismology*, 18, 497-510, 2014.

393 Elsasser, W.M.: Convection and stress propagation in the upper mantle, in: *The Application of*  
394 *Modern Physics to the Earth and Planetary Interiors*, edited by: Runcorn, S.K., pp. 223-246,  
395 Wiley-Interscience, New York, 1969.

396 Erickson, B.A., Birnir, B., and Lavallee, D.: Periodicity, chaos and localization in a Burridge-  
397 Knopoff model of an earthquake with rate-and-state friction, *Geophys. J. Intern.*, 187, 178-  
398 198, 2011.

399 Gorbunova, E.A. and Sherman, S.I.: Slow deformation waves in the lithosphere: Registration,  
400 parameters, and geodynamic analysis (Central Asia), *Russian J. Pacific Geology*, 6, 13-20,  
401 2012.

402 Gershenzon, N.I., Bykov, V.G., and Bambakidis, G.: Strain waves, earthquakes, slow  
403 earthquakes, and afterslip in the framework of the Frenkel-Kontorova model, *Physical*  
404 *Review. E*, 79, 056601, 2009.

405 Harada, M., Furuzawa, T., Teraishi, M., and Ohya, F.: Temporal and spatial correlations of the  
406 strain field in tectonic active region, southern Kyusyu, Japan, *Journal of Geodynamics*, 35,  
407 471-481, 2003.

408 Ida, Y.: Slow-moving deformation pulses along tectonic faults, *Phys. Earth Planet. Inter.*, 9, 328-  
409 337, 1974.

410 Imaeva, L.P., Imaev, V.S., and Koz'min, B.M.: Seismogeodynamics of the Aldan-Stanovoi block,  
411 *Russian J. Pacific Geology*, 6, 1-12, 2012.

412 Ishii, H., Sato, T., Tachibana, K., Hashimoto, K., Murakami, E., Mishina, M., Miura, S., Sato, K.,  
413 and Takagi, A.: Crustal strain, crustal stress and microearthquake activity in the northeastern  
414 Japan arc, *Tectonophysics*, 97, 217-230, 1983.

415 Kasahara, K.: Migration of crustal deformation, *Tectonophysics*, 52, 329-341, 1979.

416 Kissin, I.G.: Hydrological effects of deformation waves in the Earth's crust, *Geophysical*  
417 *Research*, 9, 43-52, 2008. (In Russian)

418 Kuz'min, Y.O.: Deformation autowaves in fault zones, *Izv. Phys. Solid Earth*, 48, 1-16, 2012.

419 Lee, W.H.K., Celebi, M., Todorovska, M.I., and Igel, H. (Eds): Special Issue on "Supplement.  
420 Rotational seismology and engineering applications", *Bull. Seism. Soc. Am.*, 99, 1486 p.,  
421 2009.

422 Lukk, A.A. and Nersesov, I.L.: Time-dependent parameters of a seismotectonic process,  
423 *Izvestiya Akademii Nauk SSSR. Fizika Zemli*, 3, 10-27, 1982.

424 Malamud, A.S. and Nikolaevskii, V.N.: The periodicity of Pamirs-Hindukush earthquakes and  
425 the tectonic waves in subducted lithosphere plates, *Dokl. Akad. Nauk. SSSR*, 269, 1075-  
426 1078, 1983.

427 Malamud, A.S. and Nikolaevsky, V.N.: Cyclicity of seismotectonic events in the marginal  
428 region of the Indian lithospheric plate, *Dokl. Akad. Nauk. SSSR*, 282, 1333-1337, 1985.

429 Mikhailov, D.N. and Nikolaevskiy, V.N.: Tectonic waves of the rotational type generating  
430 seismic signals, *Izv. Phys. Solid Earth*, 36, 895-902, 2000.

431 Milyukov, V., Mironov, A., Kravchuk, V., Amoruso, A., and Crescentini, L.: Global  
432 deformations of the Eurasian plate and variations of the Earth rotation rate, *Journal of*  
433 *Geodynamics*, 67, 97-105, 2013.

434 Miura, S., Ishii, H., and Takagi, A.: Migration of vertical deformations and coupling of  
435 island arc plate and subducting plate, in: *Slow Deformation and Transmission of Stress in the*

436 Earth, edited by: Cohen, S.C. and Vaníček, P., pp. 125-138, Washington, D.C. Geophysical  
437 Monograph Series, 49, 1989.

438 Nevskii, M.V., Morozova L.A., and Zhurba, M.N.: The effect of propagation of the long-period  
439 strain perturbations, Dokl. Akad. Nauk SSSR, 296, 1090-1094, 1987.

440 Nersesov, I.L., Lukk, A.A., Zhuravlev, V.I., and Galaganov, O.N.: On propagation of strain  
441 waves in the crust of southern Central Asia, Izvestiya Akademii Nauk SSSR. Fizika Zemli, 5,  
442 102-112, 1990.

443 Nikolaevskiy, V.N.: Geomechanics and fluidodynamics, Kluwer, Dordrecht, 1996.

444 Nikolaevskiy, V.N.: Tectonic stress migration as nonlinear wave process along earth crust faults,  
445 in: Proc. of 4th Inter. Workshop on Localization and Bifurcation Theory for Soils and Rocks,  
446 Gifu, Japan, 28 Sept. - 2 Oct. 1997, edited by: Adachi, T., Oka, F., and Yashima, A., 137-142,  
447 Balkema, Rotterdam, 1998.

448 Press, F. and Allen, C.: Patterns of seismic release in the southern California region, J. Geophys.  
449 Res., 100, 6421-6430, 1995.

450 Reuveni, Y., Kedar, S., Moore, A., and Webb, F.: Analyzing slip events along the Cascadia  
451 margin using an improved subdaily GPS analysis strategy, Geophys. J. Intern., 198, 1269-  
452 1278, 2014.

453 Scholz, C.H.: A physical interpretation of the Haicheng earthquake prediction, Nature, 267, 121-  
454 124, 1977.

455 Serpelloni, E., Faccenna, C., Spada, G., Dong, D., Williams, S.D. P.: Vertical GPS ground  
456 motion rates in the Euro-Mediterranean region: New evidence of velocity gradients at  
457 different spatial scales along the Nubia-Eurasia plate boundary, J. Geophys. Res., 118, 6003-  
458 6024, 2013.

459 Sherman, S.I.: Deformation waves as a trigger mechanism of seismic activity in seismic zones of  
460 the continental lithosphere, Geodynamics & Tectonophysics, 4, 83-117, 2013.

461 Sherman, S.I., Sorokin, A.P., Sorokina, A.T., Gorbunova, E.A., and Bormotov, V.A.: New data  
462 on the active faults and zones of modern lithosphere destruction in the Amur region, Doklady  
463 Earth Sciences, 439, 1146-1151, 2011.

464 Stein, R.S., Barka, A.A., and Dieterich, J.H.: Progressive failure on the North Anatolian fault  
465 since 1939 by earthquake stress triggering, Geophys. J. Intern., 128, 594-604, 1997.

466 Teisseyre, R., Takeo, M., and Majewski, E. (Eds): Earthquake source asymmetry, structural  
467 media and rotation effects, Springer-Verlag, Berlin, 2006.

468 Trofimenko, S.V.: Tectonic interpretation of the statistical model of distributions of anomalies  
469 azimuths of gravity and magnetic fields of the Aldanian Shield, Pacific Geology, 29, 64-77,  
470 2010. (In Russian)

471 Trofimenko, S.V. and Bykov, V.G.: The model of crustal block movement in the South Yakutia  
472 geodynamic testing area based on GPS data, *Russian J. Pacific Geology*, 8, 247-255, 2014.

473 Trofimenko, S.V., Bykov, V.G., and Merkulova, T.V.: Seismicity Migration in the Zone of  
474 Convergent Interaction between the Amur Plate and the Eurasian Plate, *Journal of*  
475 *Volcanology and Seismology*, 9, 210-222, 2015.

476 Trofimenko, S.V., Bykov, V.G., and Merkulova, T.V.: Space-time model for migration of  
477 weak earthquakes along the northern boundary of the Amurian microplate, *Journal*  
478 *of Seismology*, 2016a. doi:10.1007/s10950-016-9600-x

479 Trofimenko, S.V., Bykov, V.G., Shestakov, N.V., Grib, N.N., and Takahashi H.: A new insight  
480 into the nature of seasonal variations in coordinate time series of GPS sites located near  
481 active faults, *Frontiers of Earth Science*, 10, 560-569, 2016b.

482 van Dam, T.M., Blewitt, G., and Heflin, M.B.: Atmospheric pressure loading effects on global  
483 positioning system coordinate determinations, *J. Geophys. Res.*, 99, 23939-23950, 1994.

484 Wang, S. and Zhang, Z.: Plastic-flow waves ("slow-waves") and seismic activity in Central-  
485 Eastern Asia, *Earthquake Research in China*, 19, 74-85, 2005.

486 Wu, Z.L. and Chen, Y.T.: Solitary wave in a Burridge-Knopoff model with slip-dependent  
487 friction as a clue to understanding the mechanism of the self-healing slip pulse in an  
488 earthquake rupture process, *Nonlin. Processes Geophys.*, 5, 121-125, 1998.

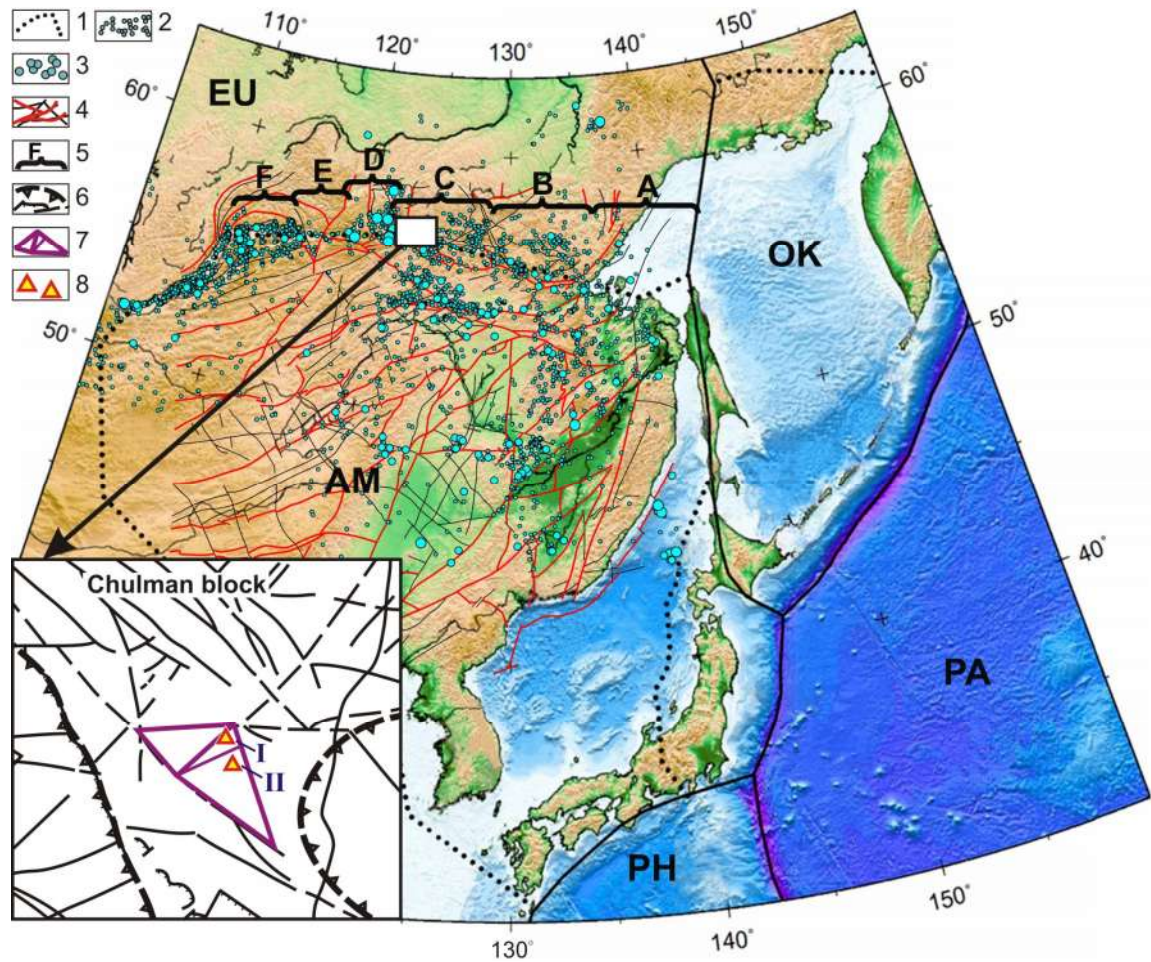
489 Yoshioka, S., Matsuoka, Y., and Ide, S.: Spatiotemporal slip distributions of three long-term  
490 slow slip events beneath the Bungo Channel, southwest Japan, inferred from inversion  
491 analyses of GPS data, *Geophys. J. Intern.*, 201, 1437-1455, 2015.

492  
493  
494  
495  
496  
497  
498  
499  
500  
501  
502  
503  
504  
505  
506  
507  
508  
509  
510  
511



512 **Figures**

513



514

515 **Fig. 1.** The distribution of earthquake epicenters in the zone of interaction between the Amurian,  
516 Eurasian and Okhotsk lithospheric plates.

517 1 – lithospheric plate boundaries: EU - Eurasian PA - Pacific, PH - Philippine, OK – Okhotsk; 2  
518 – epicenters of earthquakes with magnitude  $M>3$ ; 3 - epicenters of earthquakes with magnitude  
519  $M>5$ ; 4 – main tectonic faulting; 5 – spatial cycles of seismicity.

520 A black rectangle shows a sketch map of fault tectonics of the Chulman block, where GPS sites  
521 are located: 6 – northeast- and northwest-trending faults of different kinematics; 7 – local block,  
522 bordered by active faults; 8 – GPS sites (I – NRGR, II – NRG2).

523

524

525

526

527

528

529

530

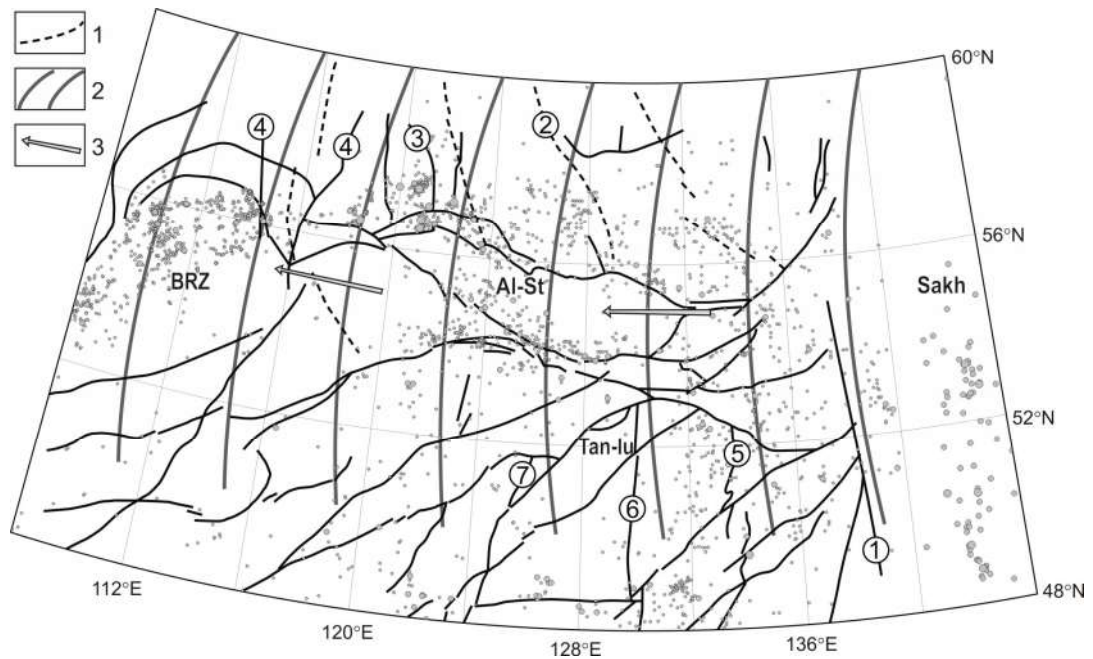
531

532

533

534





535  
536

537 **Fig. 2** The spatial distribution of seismicity in the annual cycles with respect to the strain wave  
538 fronts and meridional structures.

539 Active tectonic faulting: Tan-Lu fault zone, Aldan-Stanovoy block (Al-St) and Baikal rift zone  
540 (BRZ). Figures in the circles denote the faults: 1 - Limurchan, 2 - Tyrkanda, 3 – Temulyakit  
541 meridional faults, 4 – meridional structures of the eastern flank of the Baikal rift zone, 5 –  
542 Gastakh, 6 – West-Turanian, 7 – Levo-Minsky.

543 1 – submeridional interblock faults of the Aldan shield; 2 – strain wave fronts (Sherman, 2013);  
544 3 – the direction of seismicity maxima migration in the annual cycles and movements of the  
545 strain wave fronts.

546

547

548

549

550

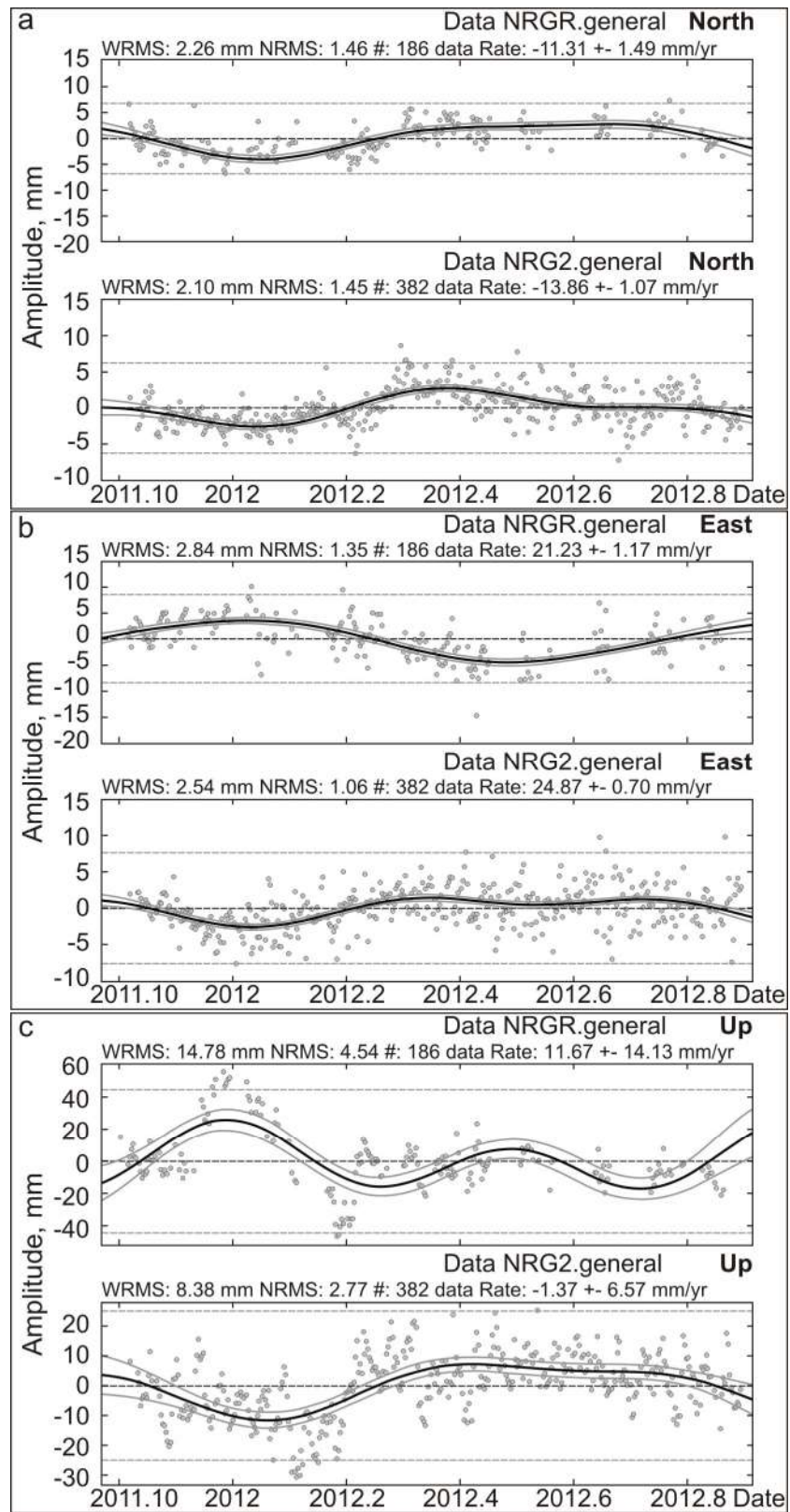
551

552

553

554

555



556

557 **Fig. 3** The dynamics of displacement components of NRGR and NRG2 station daily positions in  
 558 different directions.

559 a – for the N–S components; b – for the E–W components; c – for the vertical (Up–Down)  
 560 components.

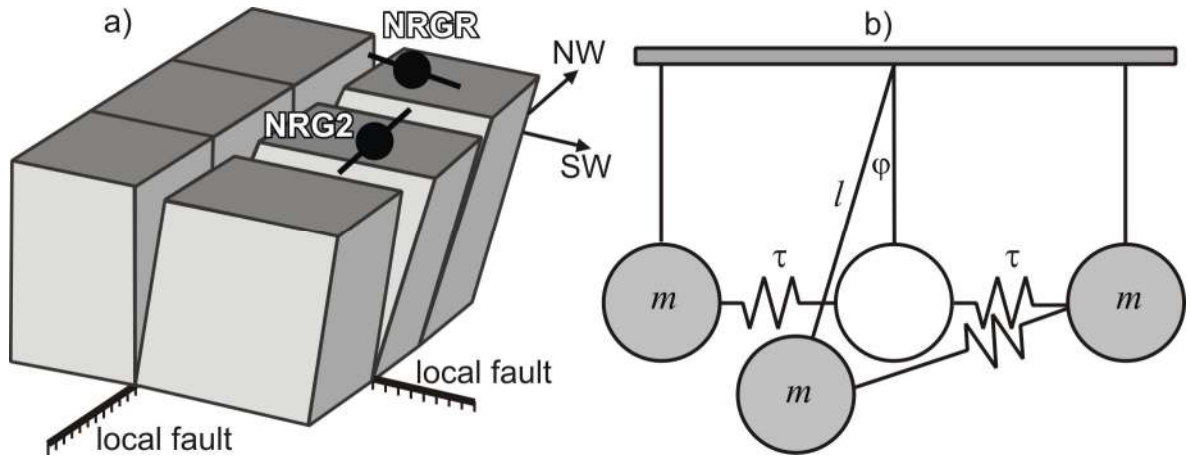
561

562

563

564

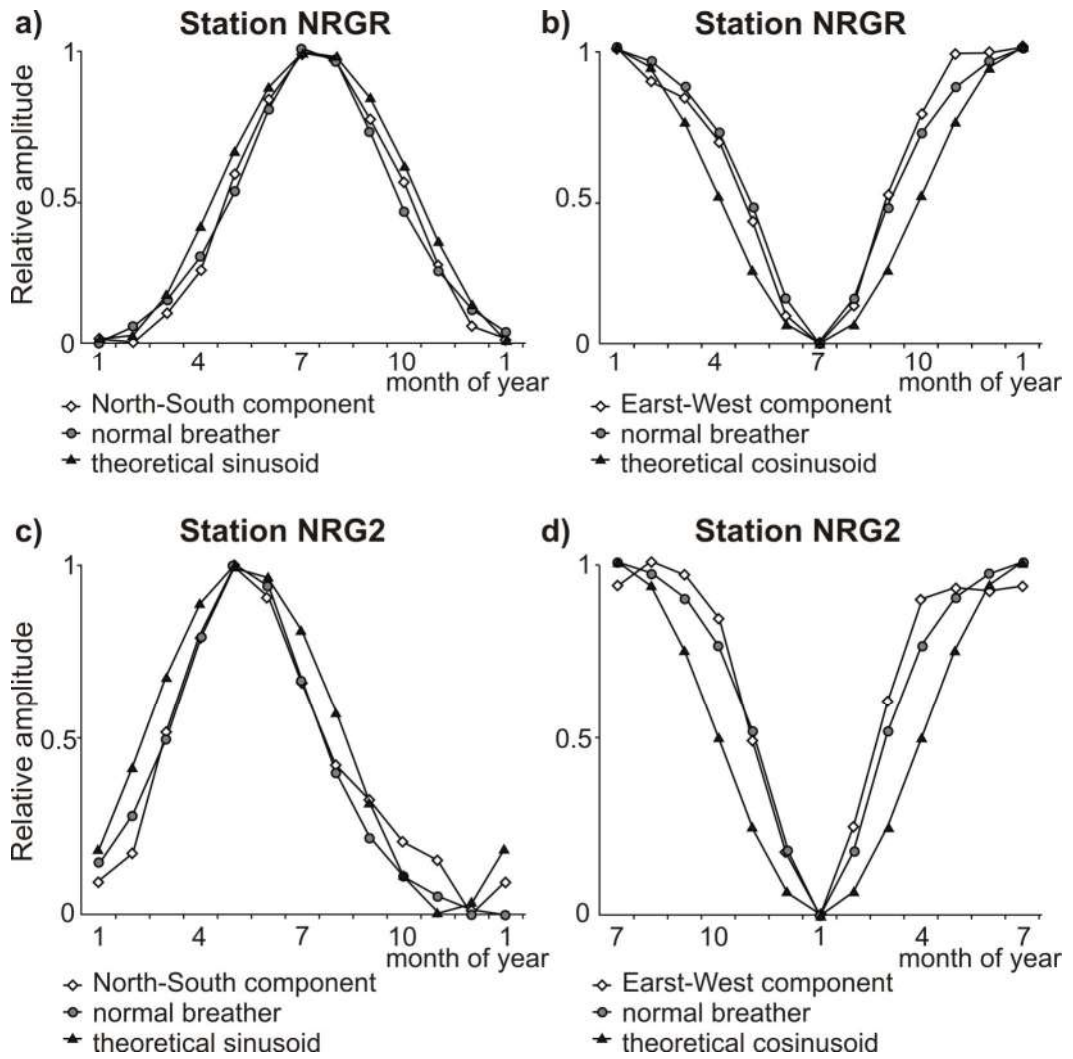
565  
566



567  
568  
569  
570  
571  
572  
573  
574

**Fig. 4** The generalized model of block movement in the vertical plane along differently oriented local faults of the hinge type due to variable vertical loading. (a) The model of block movement along NE- and NW-trending faults and schemes of the full displacement vector decomposition into components. (b) The model of block movement in the shape of coupled pendulums (notations are given in the text).

575  
576  
577  
578  
579  
580  
581  
582  
583  
584  
585  
586  
587  
588  
589



590

591 **Fig. 5** Seasonal variations of NRGR and NRG2 station positions.  
 592 Approximation of the observed displacement curves by the theoretical curves for the N-S (a) and  
 593 E-W (b) components at the NRGR site; for the N-S (c) and E-W (d) components at the NRG2  
 594 site.  
 595